Deep Resources Engineering 3 (2026) 100239

Contents lists available at ScienceDirect

Deep Resources Engineering

journal homepage: www.keaipublishing.com/en/journals/deepre/

Full length article

Insight into undercut-induced ground deformations in cave mines

Batbayar Batkhuu [a,*], Andre van As [b]

[a] Rio Tinto, Oyu Tolgoi, Ulaanbaatar 14240, Mongolia
[b] Sustainable Minerals Institute, The University of Queensland, Brisbane 4072, Australia

ARTICLE INFO

Keywords:
Undercutting
High-stress caving
Ground response to undercutting
Deformation monitoring

ABSTRACT

As underground cave mines transition to greater depths, they face the unavoidable challenge of managing stress-driven instabilities on the extraction level, particularly those resulting from high abutment stresses induced during the undercutting process. The primary objective of undercutting is to establish an adequate stope to initiate caving. However, in deep and high-stress caves, undercutting must also aim to mitigate the impact of high abutment stress effects resulting from the undercutting process. This paper primarily aims to review previous studies on undercut-induced deformation analysis. Secondly, it seeks to understand ground responses to understand the ground responses to undercutting using common displacement monitoring measurements including Multi-Point Borehole Extensometer (MPBX) and convergence pins. Three cave mines objectively selected to compare ground deformation trends and patterns during undercutting stage. Findings illustrate that the same deformation pattern observed during undercut passes over monitoring locations in all three cases and its rate and magnitude increase as undercut expands. Higher deformations during undercut stage tended to show resumption after undercutting. This highlights the importance of predicting and mitigating stress-induced deformations during undercutting in cave mines.

1. Introduction

Laubscher [1] emphasised that undercutting is a critical phase in block and panel cave mining, where the initiation of caving processes creates a sufficient undercut (UC) stope that allows for the controlled collapse of the rock mass, facilitating ore extraction. However, the UC stope also generates high abutment stresses, which can potentially compromise operational safety and infrastructure stability.

Early shallow cave mines were typically in weaker rock masses that were naturally caveable, where vertical cave propagations limited the abutment loading conditions, thereby reducing susceptibility to stress-induced damage [2]. However, rock masses exhibit high variability and are often more massive at greater depths, necessitating a larger UC area to initiate caving. The tabular shape of UC stope in high-stress environments generates significant abutment loading on the surrounding rock mass and excavations mined ahead of the UC front. Two primary loading effects in block and panel cave mining can be identified: abutment loading and cave loading (Fig. 1).

High abutment stresses generated during undercutting can exceed the strength of the rock mass, potentially leading to collapses at both the extraction and UC levels. Several recent cave mines have reported instances of stress-induced damage or collapse during the undercutting phase [2–5].

Observational and analytical approaches have been applied to assess the ground displacement in response to undercutting, and geotechnical monitoring systems are now widely implemented in mining operations to manage stress-driven collapses. These systems collect valuable spatial and temporal data, capturing fluctuations in ground response, displacements, and deformation patterns in response to undercutting and production activities. Analysing this geotechnical monitoring data provides insights into the complex interactions between rock mass and mining-induced stresses. It also helps validate empirical rules and calibrate numerical models to improve our understanding of undercutting behaviour.

This research primarily reviews previous studies that have investigated UC-induced instabilities using field monitoring data from deep and high-stress cave mines. It also presents a spatial and temporal observational analysis of the undercutting process and associated deformation monitoring data to better understand ground displacement patterns in selected case studies. By analysing monitoring data, the study aims to identify the key factors contributing to stress-driven damage, enhance the prediction of ground behaviour, and support safer, more

* Corresponding author.
E-mail address: Batbayarbatk@riotinto.com (B. Batkhuu).

https://doi.org/10.1016/j.deepre.2026.100239
Received 31 July 2025; Received in revised form 9 January 2026; Accepted 12 January 2026
Available online 15 January 2026

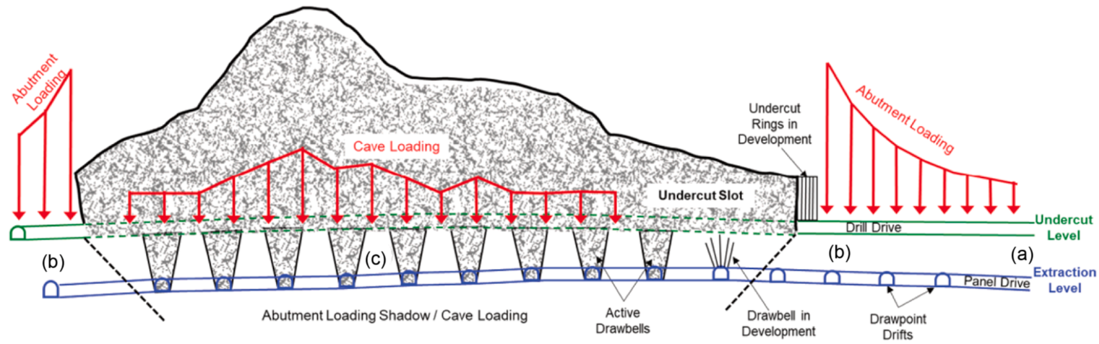

Fig. 1. The abutment and cave loading conditions in a deep cave mine: (a) in-situ; (b) abutment loading; (c) cave loading conditions [2].

effective undercutting practices in deep and high-stress environments.

2. Previous studies and selected cases

Assessments of rock mass responses to mining are inherently based on idealisations, assumptions, and simplifications due to the complexity of rock masses and the difficulty in determining their engineering properties. Therefore, observational studies are essential to verify the accuracy of predictions made by design calculations [6].

2.1. Previous studies in rock mass response to undercutting

Several examples from block and panel cave operations demonstrate how geotechnical monitoring techniques have been used to identify the primary factors contributing to instability during undercutting [7–9]. Monitoring plays a critical role in the observational method, encompassing both visual observations and instrumentation. These studies have identified distinct phases of rock mass deformation during undercutting, including:

1) the initiation phase, marked by a slow rate of deformation ahead of the UC front;
2) a high-rate or large-magnitude deformation phase as the UC passes beneath; and
3) a stabilisation phase following the completion of undercutting.

For example, A detailed investigation into rock mass response to conventional panel caving (post-undercutting) at Henderson mine was carried out by Brumleve and Maier [8]. Convergence monitoring of drawpoints revealed three distinct phases of displacement, including a rapid rate of convergence ahead of undercutting, elastic rebound during UC passes, and stabilisation after undercutting. Visual inspections of the extraction drive condition, combined with load cell monitoring, indicated that undercut advancement and the associated loading and unloading of the rock mass led to spalling and initial cracking of the drawpoint and drive lining.

Rojas [7] conducted a comparative study of conventional and pre-undercutting methods at the Esmeralda sector of the El Teniente mine. Various monitoring techniques were employed in this study, including seismic monitoring, stress measurements, borehole camera surveys, Time Domain Reflectometer (TDR), and damage mapping. Ground condition monitoring data revealed less damage was observed when employing the pre-undercut method, as the extraction level was developed in destressed ground. In-situ stress measurements at this mine level indicated that the major principal stress (σ_1) was 46 MPa while the intermediate (σ_2) and minor stress (σ_3) levels were 35 MPa and 16 MPa, respectively [10]. Stress cell monitoring at the extraction level showed that the major principal stress (σ_1) peaked at 90 MPa as the UC front approached the measurement station. This stress then decreased to less than 20 MPa directly below the UC area (Fig. 2).

Instability problems, mainly those associated with cave advancement or undercutting, have been extensively documented by Araneda and Sougarret [11] and Pardo Mella [12]. From 2001, significant collapses have been observed in the central cave area at the Esmeralda. The presence of primary lithological contacts and major geological faults also characterised this area. Whilst early collapses occurred behind the undercut front and were primarily associated with remnant pillars, collapse events from 2008 to 2010 occurred ahead of the undercut front, driven by high abutment stresses. Further analysis of the collapsed areas across the different sectors of the El Teniente Mine revealed a direct correlation between the length of the undercut front and the extent of the affected extraction area [12].

Northparkes Mines E48 block caving experienced significant stress loading conditions on the extraction level during undercutting in late

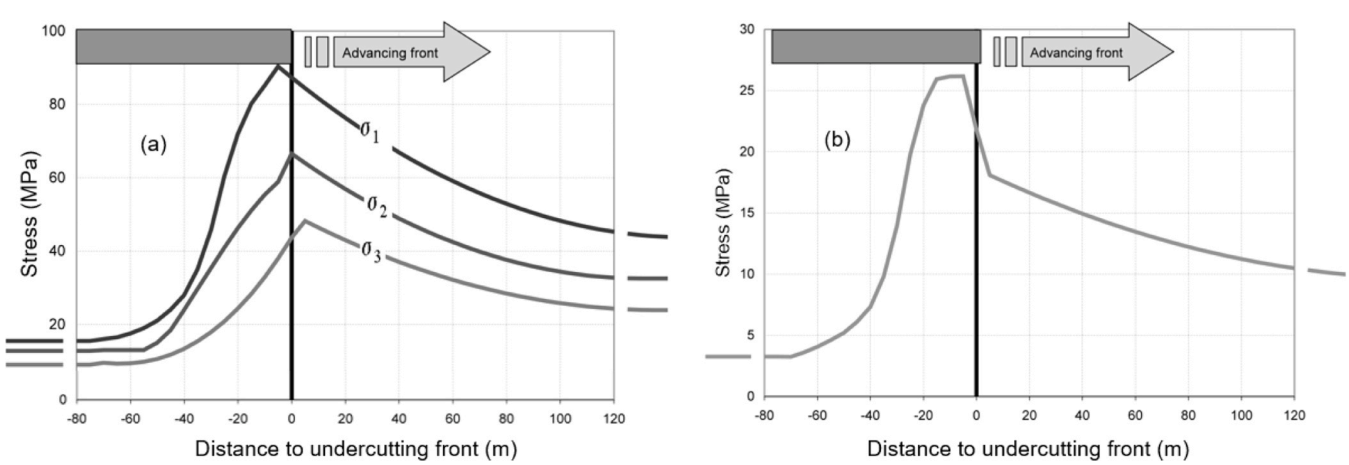

Fig. 2. Stress changes in relation to the undercut front advance: (a) principal stresses; (b) maximum shear stress [7].

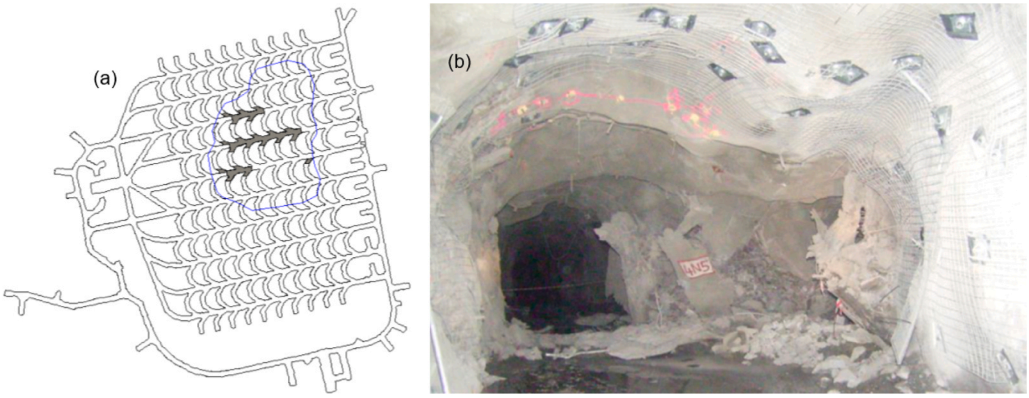

Fig. 3. (a) Northparkes Mines E48 extraction level footprint highlighting the stress-induced damage area; (b) example of pillar damage [4].

2010. The eastern region of the extraction level footprint experienced large convergence, ground support damage, and instability of the extraction level pillars due to increased abutment stresses along the UC front as the UC advanced from the west to the north-east [4]. This resulted in damage primarily in the form of horizontal deformation with pillars on the extraction level experiencing an average 3% strain or 75–200 mm convergence measured in some parts of the extraction level [4,13] (Fig. 3).

In 2015, DMLZ initiated advanced undercutting with pre-mined stubs. Previous studies by Angin et al. [14], Simanjuntak et al. [15], Napitupulu et al. [16], and Roy et al. [17] examined the UC challenges experienced at the DMLZ. Several major seismic events occurred, causing ground deformation and excavation damage on both the extraction and UC levels. The majority of the rockbursts at DMLZ occurred around abutment regions or cave boundaries, particularly ahead of the active UC front. Back analysis indicated that the primary causes of rockbursts were significant lag and delays in undercutting [14].

The prominent risk of mining at depth is the increased in situ stress magnitude, while the excavation and the cave development create greater induced stress, leading to an environment of increased ground deformation and rockbursts. Brittle failures, such as spalling and strainbursts, were prevalent due to the presence of massive, strong rock masses that were subjected to high abutment stress conditions. According to Roy et al. [17], a near-constant state of instability in the rock mass surrounding the mine drifts can be attributed to ongoing abutment loading and undercut advancement, with the extraction ratio and rock mass characteristics identified as the most influential factors. These findings suggested that maintaining a consistent progression of the UC front is critical for preventing rockbursts.

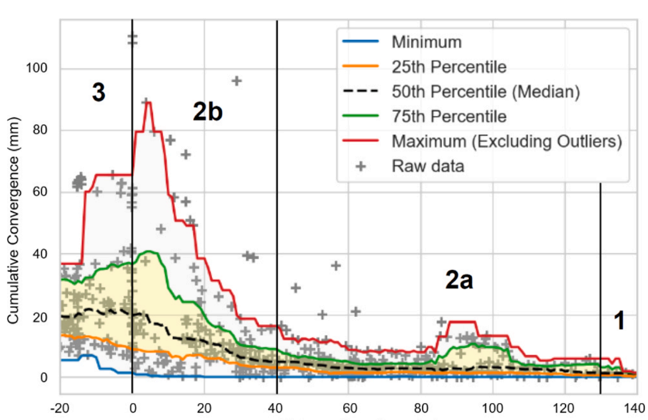

Fig. 4. The general trend of rock mass response to UC advance based on convergence monitoring at the DMLZ [18].

The observational analysis of the rock mass response to undercutting was conducted by McMillan [18] at the DMLZ cave mine. This study applied a simple two-factor empirical susceptibility mapping approach, considering intact rock strength (UCS) and distance to the UC front. Several monitoring datasets were used, including MPBX, convergence, borehole camera (BHC) surveys, and 3D LiDAR scanning. As illustrated in Fig. 4, the general rock mass response to the UC advance was categorised into three main zones:

1) Pre-undercutting (in-situ stress zone): Greater than 130 m from the cave front
2) Abutment stress from undercutting (130 m to 0 m from the cave front), divided into:
   a. Deformation initiation: 40 m to 130 m from cave front
   b. High-rate deformation zone: 0 m to 40 m from the cave front
3) Stress relaxation: After the UC front has passed over the monitoring location

An extensive study of undercutting in deep caves (below 1,000 m) at Cadia operations - including Ridgeway Deeps (RWD), Cadia East Panel Cave 1, and Panel Cave 2 – was conducted by Lett [9]. Table 1 outlines the key parameters of each mining footprint and the associated undercutting challenges.

It should be noted that in the hybrid post-undercut method, some of the extraction drives – typically every second or third – and their associated drawbells are developed after undercutting. This approach creates a stress shadow that facilitates safer drawbell development and allows for the formation of larger pillars at the stress abutment and UC front, thereby improving geotechnical stability.

Both undercutting approaches generate stress abutments; however, their characteristics depend on mining geometry, stress magnitude and orientation, geological conditions, mining sequence and ground support capacity. Previous studies have highlighted that the most influential

Table 1
Cadie operations, underground mining footprint key parameters and UC response from Lett [9].

Mine name	Undercut method	Undercut area (m^2)	Undercut response
Ridgeway Deeps	Advanced	85,000	Rock mass deformation on lithological units/faults
Cadia East PC1	Hybrid post	73,400	Strainbursting on intrusive contacts, UC pillar deformation impacting production holes
Cadia East PC2-S1 and PC2-S2	Hybrid post converted to advanced	123,600	Brittle rock mass failure Strainbursting on intrusive contacts and rockbursting
Cadia East PC2-S3	Post converted to hybrid	136,000	

Table 2
Key UC parameters for the selected cave mines.

Cave mine	Depth (m)	UC method	Inner-level spacing (m)	Drawpoint spacing (m)	UC front shape	UC front length (m)	UC ring profile
OTP0	1,300	Advanced	17	31 × 18	Straight	275	Narrow-Incline (Big V)
DMLZ (PB1N)	1,700	Advanced	9–17	30 × 20	Concave, straight	400–500	Narrow-Incline
Northparkes Mines E48	581	Post	17	30 × 18	Straight	280	Flat

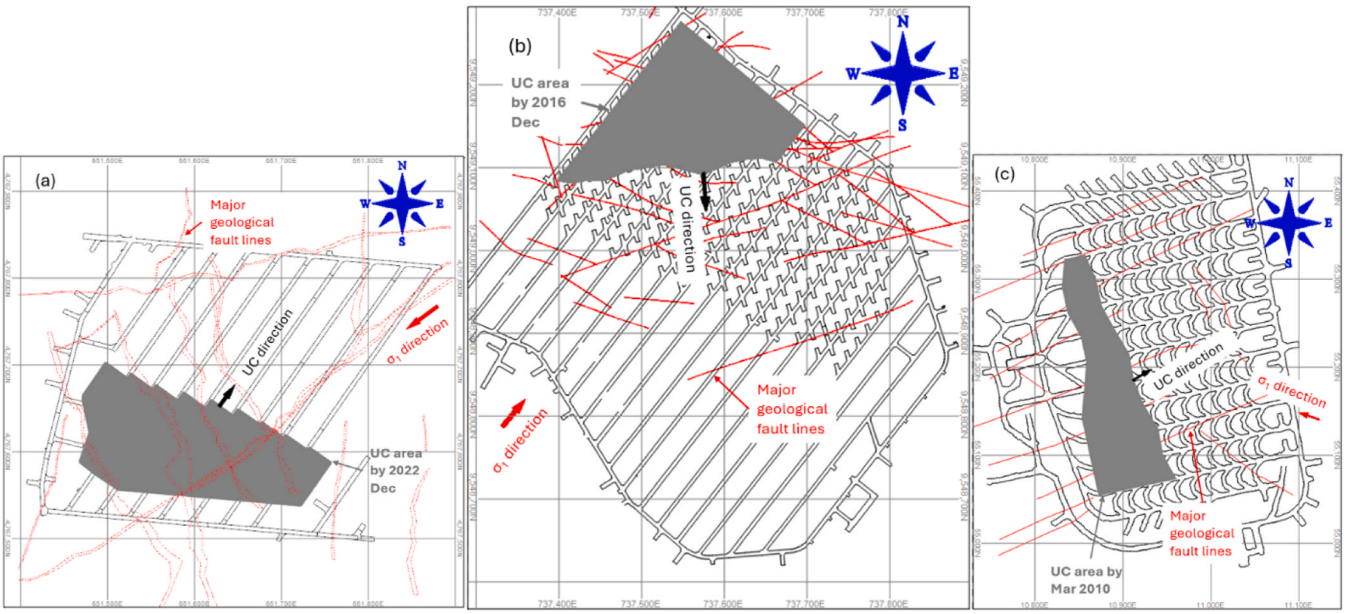

Fig. 5. Progress of undercutting for the selected cases: (a) OTP0; (b) DMLZ; (c) E48, shown relative to the extraction level as-built, geological structures, and the major principal stress direction.

factors include the size of the UC area, the length of the UC front, the UC rate, and geological structures. Structural features - such as intrusive contacts, stress-induced fracturing, and faults - should be assessed early using diamond drilling to evaluate the risk of dynamic failures, such as strainbursts and rockbursts, particularly during the UC and cave propagation phases. The following case studies aim to identify ground deformation patterns and trends at the extraction level during undercutting, and how these key parameters influence such deformations.

Table 3
Representative geotechnical rock mass parameter.

Geotechnical domain	UCS (MPa)	RMR*	Q'
OTP0 [19]			
BiGd (Low vein)	115.4	46	6.0
BiGd (High vein)	80.4	44	5.6
QMD (Advanced argillic)	55.7	45	6.2
QMD (Intermediate argillic)	78.4	43	4.3
QMD (Phyllic, low vein)	96.5	44	4.8
QMD (Phyllic, high vein)	108.8	43	5.2
QMD (other)	94.1	45	5.8
VA	72.2	44	4.5
IGN	77.5	46	3.8
DMLZ [15,17,18]			
Te Diorite	160	84	48
Hornfels	180	78	78
Exoskarn	135	80	40
E48 (L, Snyman, personal communication, September 6, 2023)			
BQM	120	77	-
Volcanic	118	76	-
Porphyry	160	-	-

* Note: The Rock Mass Rating (RMR) systems used across the cases were not consistent: OTP0 applied the classification system for mine design by Laubscher [20], DMLZ and E48 used the RMR system by Bieniawski [21].

2.2. Case studies description

Three recent cave mines were selected for detailed data analysis based on data availability and the undercutting method used. The general geotechnical settings of these mines, along with previous undercutting studies, associated challenges, and design modifications, are discussed. The key UC parameters for the selected cave mines are summarised in Table 2 and illustrated in Fig. 5.

Regarding undercutting, the primary difference among the three cases is the UC method used: DMLZ and OTP0 employed advanced undercutting, while E48 applied post-undercutting. It should be noted that the DMLZ also implemented pre-mined stubs on the extraction level, as mentioned earlier.

Additionally, all three cases encountered significantly different geotechnical conditions. The main differences include:

- Operating depth:
  - o DMLZ is located approximately 1500–1800 m below the surface, making it one of the world's deepest panel cave operations.
  - o OTP0 is located at a depth of around 1300 m, also considered a deep block cave.
  - o E48, by contrast, is relatively shallow at 581 m below the surface.
- Rock mass characteristics and stress regime:
  - o DMLZ and E48 are hosted in stronger, more massive rock masses.
  - o OTP0, however, is situated in a weaker rock mass that is moderately to highly fractured. Its strength is highly dependent on confinement: low confinement results in low intact strength, while high confinement increases strength.

At OT, the dominant rock types within the P0 footprint include an easterly-dipping sequence of volcanic strata, Quartz Monzodiorite (QMD), and Biotite Granodiorite (BiGd) intrusive rocks. The

Table 4
The principal stresses for the selected cases.

Principal stress	Magnitude (MPa)	Trend (°)	Plunge (°)
OTP0 [19]			
σ_1	57.8	00	055
σ_2	34.5	00	145
σ_3	27.2	90	058
DMLZ [15,17]			
σ_1	60	040	22
σ_2	40	215	68
σ_3	30	309	02
E48 (L, Snyman, personal communication, September 6, 2023)			
σ_1	41.0	-	290
σ_2	20.0	-	022
σ_3	12.0	-	165

stratigraphically lowest units consist of basalt flows and Augite Basalt (VA), overlain by dacite tuff, breccia, and Ignimbrite (IGN).

At DMLZ, the dominant geological domain is competent, massive diorite, characterised by limited-persistence vein systems and widely spaced, often healed or partially healed, large-scale faults.

E48 features a stronger porphyritic orebody composed primarily of Biotite Quartz Monzonite (BQM) and volcanic host rocks.

Table 3 summarizes the representative geotechnical parameters for dominant geotechnical domains in each case.

Table 4 presents in situ stress measurements at the extraction level of the selected cases, based on available data sources.

Based on rock mass characteristics and stress conditions, there is significant variability in the dominant failure mechanisms across the selected cases. Despite both OTP0 and DMLZ are located in deep, high-stress environments, they exhibit different failure behaviours. OTP0 experiences severe squeezing failure due to a moderately to highly fractured and faulted rock mass. In contrast, DMLZ is characterised by strainbursting, attributed to its massive and stronger rock mass. At E48, although the rock mass is similarly massive and strong, the environment is relatively shallower and subject to lower stress compared to the other two cases. Here, localised brittle failures and block movements are more prevalent.

3. Methodology

The primary objective of the data analysis is to assess ground deformation and excavation stability during the undercutting stage. Both spatial (displacement contouring) and temporal (displacement change over time) analyses were performed to identify zones of significant deformation, which vary depending on site-specific characteristics, undercutting progress, and other key parameters.

Two key datasets will be utilised: UC ring blasting data and deformation monitoring data. The UC ring blasting data will be used to determine the UC advancement rate, the shape of the UC front, and the distance from the UC front to each monitoring location over time.

3.1. Deformation monitoring techniques

Ground deformation can be measured using various monitoring techniques. Among these, convergence pin (Tape extensometer) and MPBX monitoring are widely used due to their simplicity and reasonable accuracy. Convergence monitoring served as the primary deformation monitoring method for the studied cases, while MPBX instruments were installed at regular intervals across the extraction level in the OT-P0 case. The continuity and frequency of these measurements will be evaluated before processing with further data analysis.

3.1.1. Convergence pin

For the three selected mines in this study, two mines, the OT-P0 and the DMLZ-PB1N, utilised 2-point convergence measurements, while NPE48 employed 3-point convergence. This method offers a convenient and straightforward way to assess excavation closure, though it requires manual data collection. Convergence stations (anchor points) can be installed at regular intervals, usually 10–20 m apart, at extraction and UC levels. The steel measuring tape of the extensometer can be stretched between two anchor points on opposite sides of the excavation tunnel. The distance between the anchor points is measured by summing the reading at the punched hole on the tape and the digital gauge reading.

Convergence data collected during undercutting were compiled from three studied cases, and the frequency of measurements was evaluated. In all three cases, convergence pins were installed at every extraction pillar, with an average spacing of 20 m. Although convergence can be measured at any desired frequency, monitoring in these cases was usually conducted weekly. For areas with high convergence rates, measurements were taken more frequently up to daily, while in relatively stable conditions, the frequency was reduced to monthly. The overall frequency of convergence monitoring was consistent, with most measurements in the OTP0 and E48 cases taken within a week. Approximately half of the convergence measurements at DMLZ were taken at intervals longer than a week or were interrupted. This inconsistency may be attributed to strainburst-related failures, which had a greater impact on convergence pin damage. Fig. 6 illustrates the frequency of convergence measurement at the selected cases.

3.1.2. Multi-point borehole extensometer (MPBX)

The International Society for Rock Mechanics and Rock Engineering [22] classifies extensometers equipped with more than two anchorage points as MPBX. These instruments are pivotal in measuring ground movement induced by various geological and engineering activities (e.g., undercutting). There are various types of borehole extensometers, including rod, wire, and probe types. In underground mining, fibreglass rod extensometers with electrical sensors are primarily used because they allow for rapid and remote readings and can be integrated into automatic data acquisition systems. Movement of each anchor point induces a measurable change in resistance across the fibreglass rods within the MPBX. This resistance variation is subsequently converted into a voltage difference relative to a standard reference voltage. Displacement is then quantified based on the ratio of these voltage

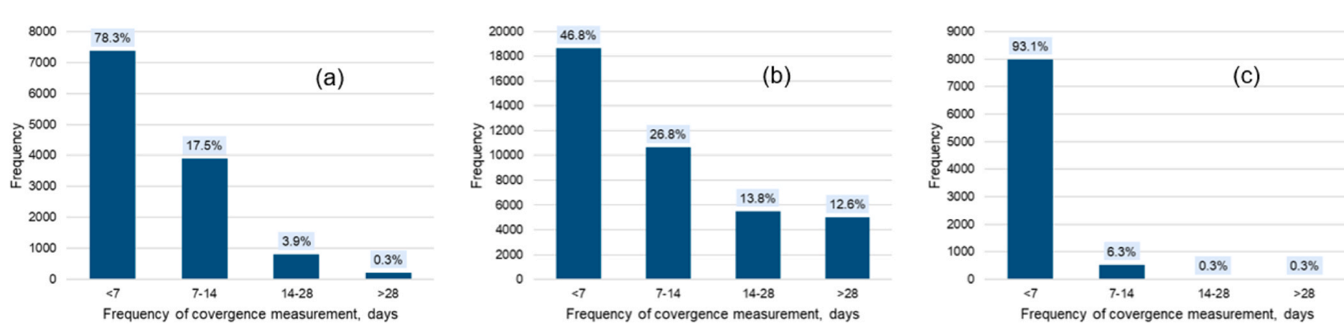

Fig. 6. The frequency of convergence measurement at the selected cases: (a) OTP0; (b) DMLZ; (c) E48.

readings.

Although MPBXs can be installed in any orientation, they are typically placed vertically or horizontally to measure ground movement in excavation backs and sidewalls. The installation process and detailed instrumentation specifications are readily available in the manufacturer's guide [23]. MPBX monitoring data provided from OTP0 is based on six anchor points positioned at depths of 0.8 m, 1.5 m, 2.5 m, 4.0 m, 7.0 m, and 10,0 m, and a head at the borehole collar (Fig. 7).

3.2. Data cleaning

Before conducting the observational data analysis, convergence and MPBX data were visually inspected and cleaned of all erroneous data measurement points. Displacement monitoring data may contain measurement noise or anomalies resulting from inaccuracies in instrumentation, environmental factors, or measurement errors. These anomalies often appear as unexpected spikes or drops in the displacement patterns over time, as illustrated in Fig. 8 by the red dotted circles.

Simple exponential smoothing with incremental filtering was chosen to objectively address these anomalies, thereby improving the continuity of monitoring data whilst still retaining the main displacement trend. The primary aim of this study was to investigate ground displacement trends and patterns during undercutting.

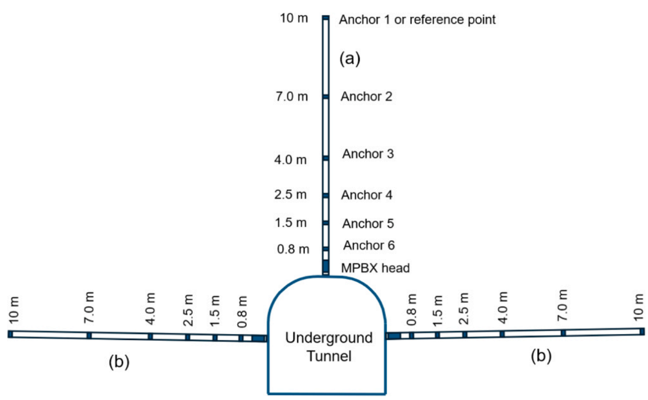

Fig. 7. Schematic showing MPBX installations in the excavation back (a) and sidewalls (b), including head details and anchor depth configuration.

3.2.1. Exponential smoothing

Exponential smoothing is one of the time series forecasting methods used to predict future values based on past observations and other inputs. The exponential smoothing is given in Eq. (1).

Eq. (1) Simple exponential smoothing

$$F_{n+1} = \alpha \times Y_n + (1 - \alpha) \times F_n \tag{1}$$

F: Forecasted value

Y: Actual (observed) value

n: Time periods for measurement taken, $n > 0$

α: Smoothing factor, and $0 < \alpha < 1$

This method is particularly useful because it incorporates both actual and forecasted values. A higher α value (smoothing factor) places more weight on actual values, resulting in a closer fit to the data, whilst a lower α value gives more emphasis to previously forecasted values, leading to a smoother but potentially less accurate fit. In practice, typical values for α range from 0.2 to 0.4. A range of α values was tested, and the smoothed values were visually compared to actual displacement over time. After visually evaluating various smoothing factors, an α value of 0.4 was selected for convergence measurements and 0.075 for MPBX data. These values were chosen because they effectively removed significant anomalies whilst also maintaining a closer fit with the actual values.

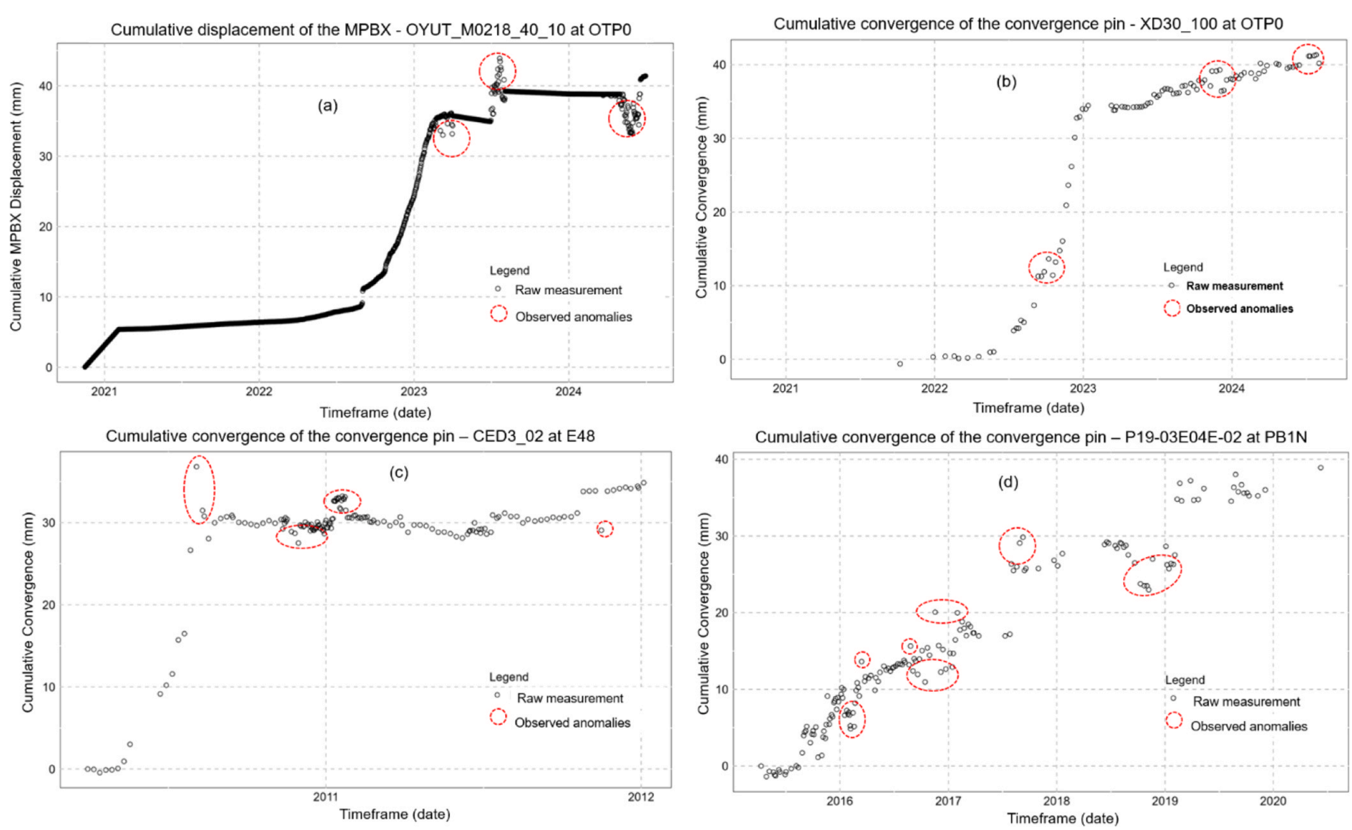

Fig. 8. Examples of raw displacement measurements with visually presented anomalies: (a) OTP0 – MPBX displacement; (b) OTP0 – convergence; (c) E48 – convergence; (d) PB1N – convergence.

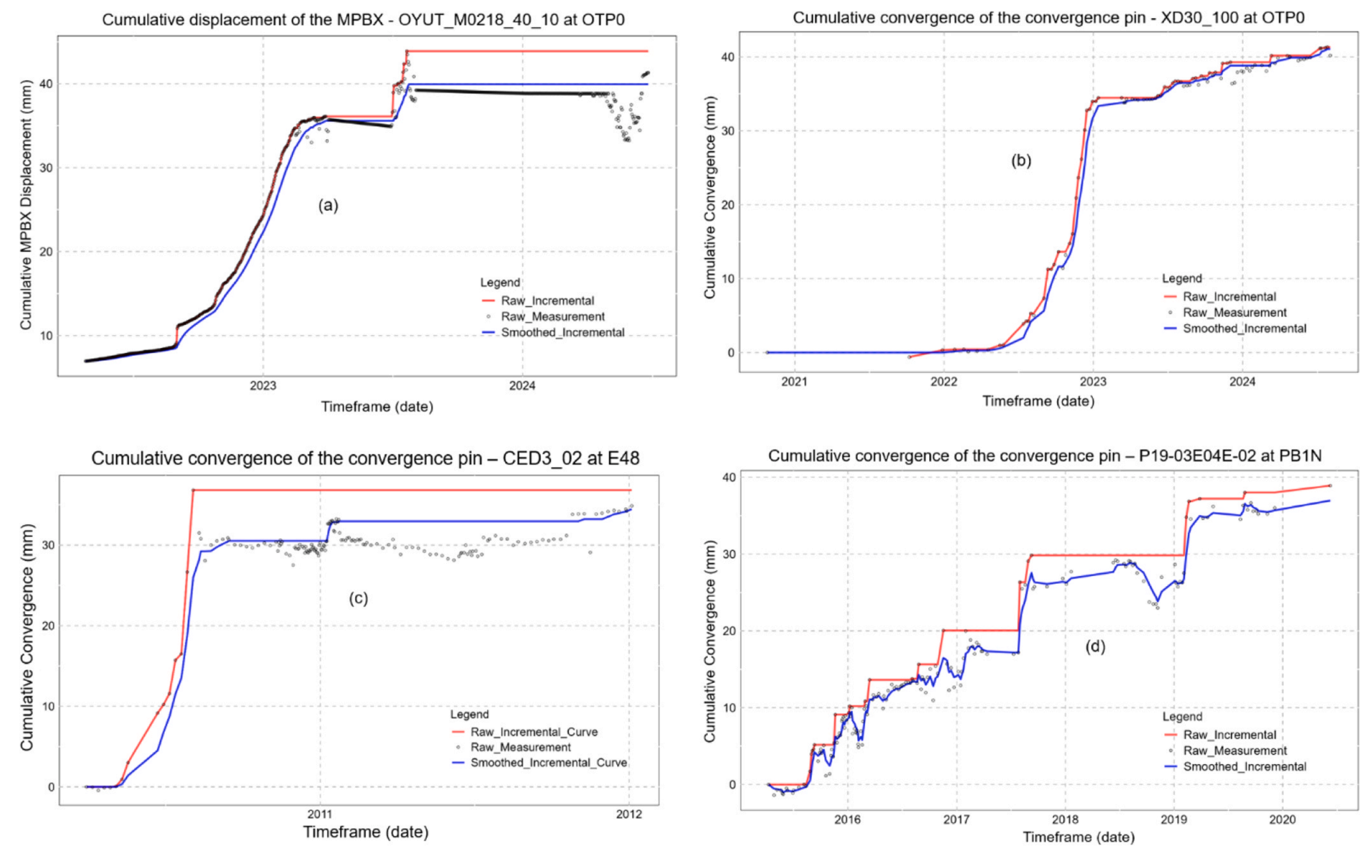

Fig. 9. Examples of incremental filtering application on smoothed and raw displacement measurement: (a) OTP0 – MPBX displacement; (b) OTP0 – convergence; (c) E48 – convergence; (d) PB1N – convergence.

3.2.2. Incremental filtering

Displacement or convergence measurements should exhibit a cumulative trend over time because they indirectly measure cumulative rock mass deformations. However, even after applying exponential smoothing, some decreasing values may still be present. To address this, an incremental filtering approach is used to assess displacement variation during undercutting and to remove any decreases in the cumulative displacement measurement data. A displacement value is included in the filtered dataset only if it is greater than or equal to the previous measurement. After anomalies are removed using incremental filtering, the

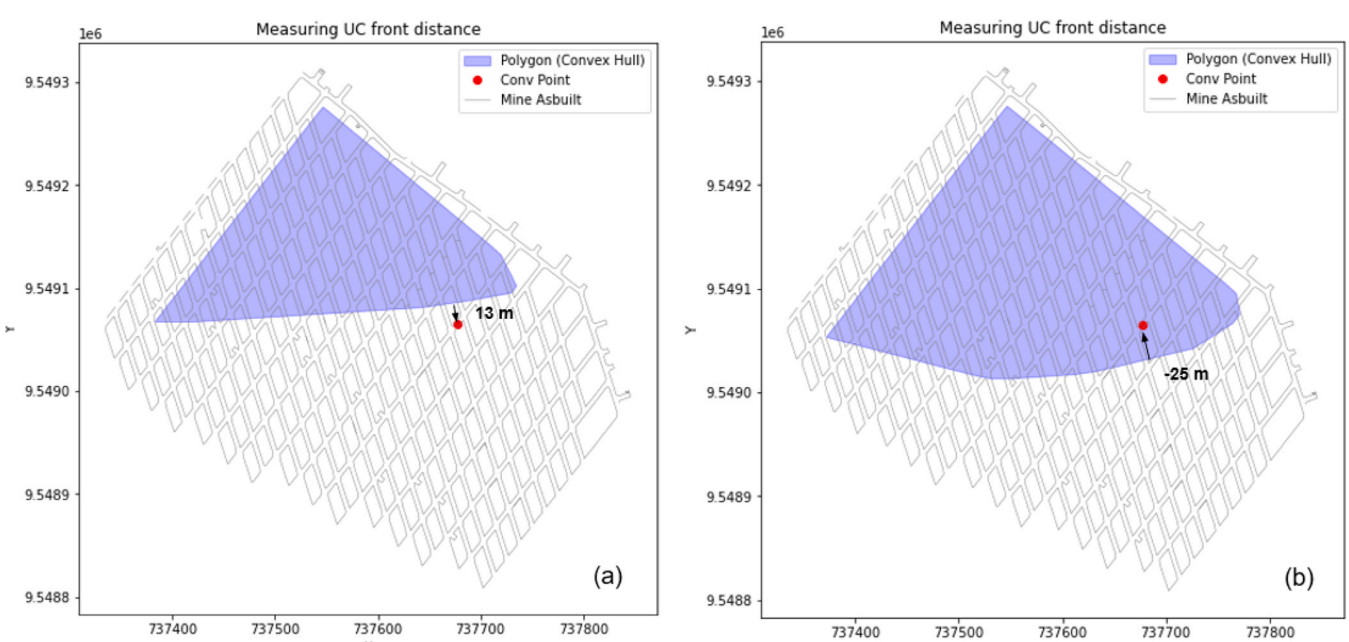

Fig. 10. Measuring the UC front distance to the monitoring point using the convex hull polygon method: (a) measurement ahead of the UC front; (b) measurement after undercutting. Note: the footprint 'as-built' represents a mine plan, not actual mined extraction drives at that time.

displacement curve becomes cumulative. Fig. 9 compares the filtered curves between smoothed (cleaned) and raw measurements, demonstrating that incremental filtering after smoothing produces a more realistic representation.

3.3. Spatial and temporal analysis

This study investigates ground responses to undercutting through spatial and temporal analysis of rock mass displacement data from selected deep cave mines. The analysis is based on cleaned and visually inspected monitoring datasets, combined with UC ring blasting information.

The spatial analysis focuses on displacement contouring to explore the distribution of deformation across the mining footprint and its correlation with UC geometry. The temporal analysis examines how displacements evolve over time, identifying deformation trends and critical changes associated with stress redistribution. Together, these approaches aim to improve understanding of UC-induced ground behaviour and support the optimisation of UC sequences to reduce stress-related damage.

Finally, visual observations and simple correlation will be applied to assess the relationship between displacement changes and proximity to key features, such as UC delays, lead-lag distances, and major fault lines. The previous studies identified four key parameters that most strongly affect ground response during undercutting: UC front geometry, UC method, UC rate, and the presence of major geological structures.

3.3.1. UC front distance to the monitoring point

The distance between the UC front and the extraction level monitoring point is a key factor in investigating the ground response to undercutting. This distance can be measured calculating the closest distance from the monitoring point to the UC area using a convex hull polygon created from the coordinates of the blasted rings. Positive values indicate that the UC has not passed over the location of the monitoring station, and negative values indicate that the UC has passed over (Fig. 10).

3.3.2. Displacement contouring

Convergence and MPBX monitoring instruments are typically installed at regular intervals, usually in every extraction pillar, with data collected consistently. This data enables us to identify areas of concentrated rock mass displacement across the footprint. Displacement contouring is a simple and widely used method for visualising spatial variations in rock mass displacement data in block and panel caving operations. One of the most widely used approaches for contouring is grid-based mapping, as employed by the Surfer software tool. Surfer has several options for gridding methods, including Kriging, Radial Basis Function, Nearest Neighbour, Natural Neighbour, Linear Interpolation, and Data Metrics [24].

However, Kriging is one of the more flexible and accurate gridding methods; applying the Kriging method can be slower than the other methods due to the high computational cost of variogram recalculations required for real-time displacement monitoring data, and it can also extrapolate grid values beyond the range of the data. Various methods were tested using MPBX displacement data for the OT-P0 case, and the Radial Basis Function (RBF) Interpolator method proved the most robust.

An advantage of this method is that it can run unsupervised when applying the Linear algorithm. RBF interpolation is combined with the Fast Nearest Neighbour (FNN) Search Algorithm to accommodate sparsely distributed measurements, aiming for a balance between local precision and interpolation smoothness while avoiding extensive extrapolation into areas without nearby data. The contouring process is carried out using the SciPy package in Python.

The FNN search restricts the influence of interpolation by selecting the number of neighbours (K) within a defined radius (R), creating contours that reflect more localised data. The search radius controls how quickly each neighbour's influence decreases with distance, and it is recommended to set this radius slightly larger than the average spacing between neighbouring points. For example, in selected sites, where the average distance between convergence points is 20–30 m, a radius slightly higher than 30 m was chosen for contouring.

The number of neighbours, K, is selected based on data density and variability. With sparsely sampled convergence monitoring data that may exhibit high variability, a smaller K value is suggested to enhance local accuracy and avoid excessive smoothing.

RBF interpolation with a linear function is applied using only the grid points that fall within the valid radius. The interpolated value at each grid point within the defined distance is computed by the linear RBF function using the original measured points (Eq. (2)).

Eq. (2) The distance for each neighbour point

$$d_i = \sqrt{(x_{\text{grid}} - X_i)^2 + (y_{\text{grid}} - Y_i)^2} \tag{2}$$

d_i: The distance between the grid points and the neighbour

$X_i,\ Y_i$: Original data points

$x_{\text{grid}},\ y_{\text{grid}}$: Grid point where interpolation is performed

The interpolated value, Z_{grid}, at each grid point, is a weighted sum of neighbouring values within the defined radius (Eq. (3)).

Eq. (3) The interpolating value at each grid point

$$Z_{\text{grid}} = \sum_{i=1}^{N} \lambda_i \times (d_i) \tag{3}$$

Z_{grid}: The interpolated value at the grid point

λ_i: The weights associated with each known point, which are determined based on solving the RBF interpolation system

If the nearest neighbours of a grid point are beyond the defined radius, the grid point is assigned an NA (no interpolated value), ensuring that the method does not extrapolate in areas without nearby data, which is common in sparse data regions.

A major concern with displacement contouring is that some high-deformation or damaged areas may not be captured due to discontinued convergence measurements in these zones due to rehabilitation activities or safety concerns. To fill this gap, known rehabilitation (rehab) or PSM-implemented areas need to be overlaid with the layers used in displacement contouring.

3.3.3. Detecting displacement rate changes

As highlighted in Section 3.1, UC studies have shown that displacement monitoring data exhibit distinct patterns during undercutting, including initiation, high-rate deformation, and stabilisation. Identifying and analysing these movement zones is key to understanding ground responses to undercutting. This section outlines the methodology for defining distinct movement zones based on displacement rates for selected cases.

Various thresholding methods can be used to define significant slope changes in cumulative displacement curves. The three main approaches are:

Fixed Thresholds: A predefined displacement rate value (site-specific). If the slope exceeds this value, it is considered a deflection or breakpoint. However, this method is sensitive to dataset variability and may miss significant changes if displacement rates do not reach the predefined levels.

Standard Deviation (SD) Thresholds: The threshold is set as a multiple of the dataset's standard deviation. This approach accounts for data variability but assumes a normal distribution, often not in displacement data.

Quantile-Based Thresholds: A threshold is determined based on the distribution of displacement rate changes (e.g., 90th or 95th percentile). This method is more robust for skewed datasets with high variability, ensuring that significant changes are data-driven rather than

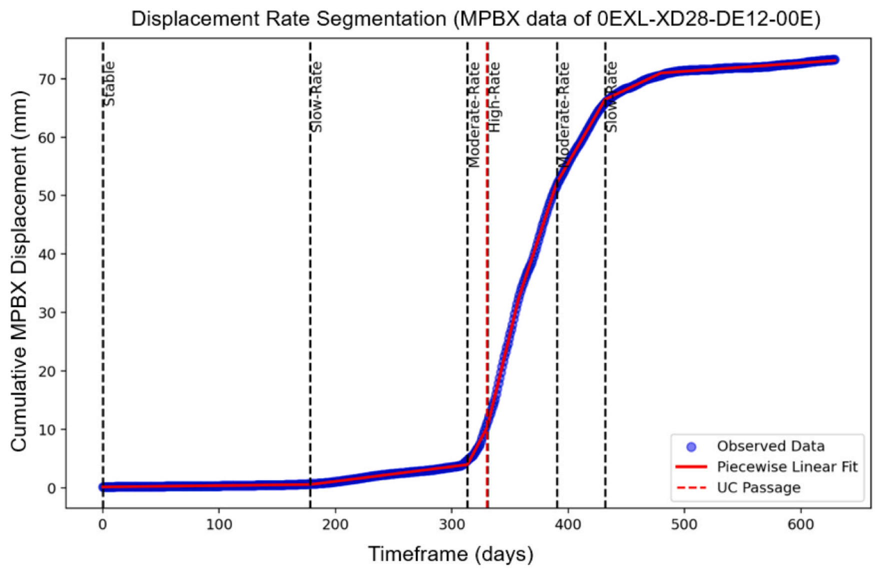

Fig. 11. An example of a PWL curve with rate change points of displacement segments.

arbitrarily defined.

This study employed a quantile-based threshold due to the high variability of displacement data, which has a predominantly skewed distribution. The methodology for detecting breakpoints and segmenting the dataset into displacement zones involves the following steps:

1) **Calculating slopes (first derivatives)**
   The displacement rate is computed as the slope between two consecutive measurements (Eq. 4).
   Eq. (4) Slope calculation

$$m_i = \left(\frac{y_{i+1} - y_i}{x_{i+1} - x_i}\right) \tag{4}$$

   m_i: The slope between two consecutive points
   x_i: Date (time in days)
   y_i: Measurement (cumulative convergence)
2) **Calculate Slope Changes (Second Derivatives)**
   Slope changes are calculated as the difference between consecutive slopes. Significant changes can be determined using the threshold. If slope change exceeds the determined threshold value, a significant change is introduced (Eq. (5)).
   Eq. (5) Slope change calculation

$$\Delta m_i = (m_{i+1} - m_i) \tag{5}$$

   Significant changes $= \{i||\Delta m_i| > T\}$
   Δm_i : The slope changes
   T: The Threshold
3) **Segment Data Using a Piecewise Linear Fit Model**
   After identifying breakpoints, the dataset is divided into segments. A piecewise linear model (PWLF) is used to optimise the location of breakpoints, ensuring a continuous best-fit function [25]. A Python library of PWLF is applied to the data to extract optimal breakpoints for segmentations (Eq. (6)).
   Eq. (6) Piecewise linear model fit

$$y = m_i x + b_i, \quad x \in [x_i, \ x_i + 1] \tag{6}$$

   y: Linear segment
   m_i: The slope of segment i
   b_i: The intercept
   $\in [x_i, x_i + 1]$: represents a segment defined by two consecutive breakpoints

Finally, the dataset is segmented using two consecutive breakpoints as the start and end of each displacement zone, allowing the computation of slope gradient (displacement rate), total displacement, time, and UC front distance. An example of a PWL model with detected change points (indicated by a vertical dashed line) of different segments is shown in Fig. 11.

Based on the displacement change analysis, high-rate displacement zones can be identified for each case. The convergence rate and magnitudes during different undercutting stages will have been calculated within the time window of these high-rate displacement zones for each monitoring station.

4. Results

Data analysis investigated displacement distributions and patterns across various monitoring locations in relation to the UC front position. It incorporates visual contouring of displacements, cumulative displacement curves, and identification of deformation phases through analysis of displacement rate changes. Given the typical monitoring frequency of 1–2 weeks, monthly displacement contours were generated using both cumulative and averaged daily displacement rates. The daily rate was calculated from the average of the three most recent measurements, providing a representative estimate. Dynamic legends were applied to highlight areas of concentrated high displacement rates, thereby improving visual interpretation.

4.1. Visual observation of displacement contouring and cumulative curves

Visual observations from monthly displacement contouring and cumulative displacement curves, plotted against UC advance and color-coded by the monitoring point's location relative to the UC initiation point, revealed that high displacement zones consistently formed around the advancing UC front (Fig. 12).

Combined cumulative displacement curves showed that the highest displacements occurred when the UC front passed over the monitoring locations. A noticeable resumption in displacements after undercutting was observed in the OTP0 and E48 cases, while significant early displacements were recorded at PB1N.

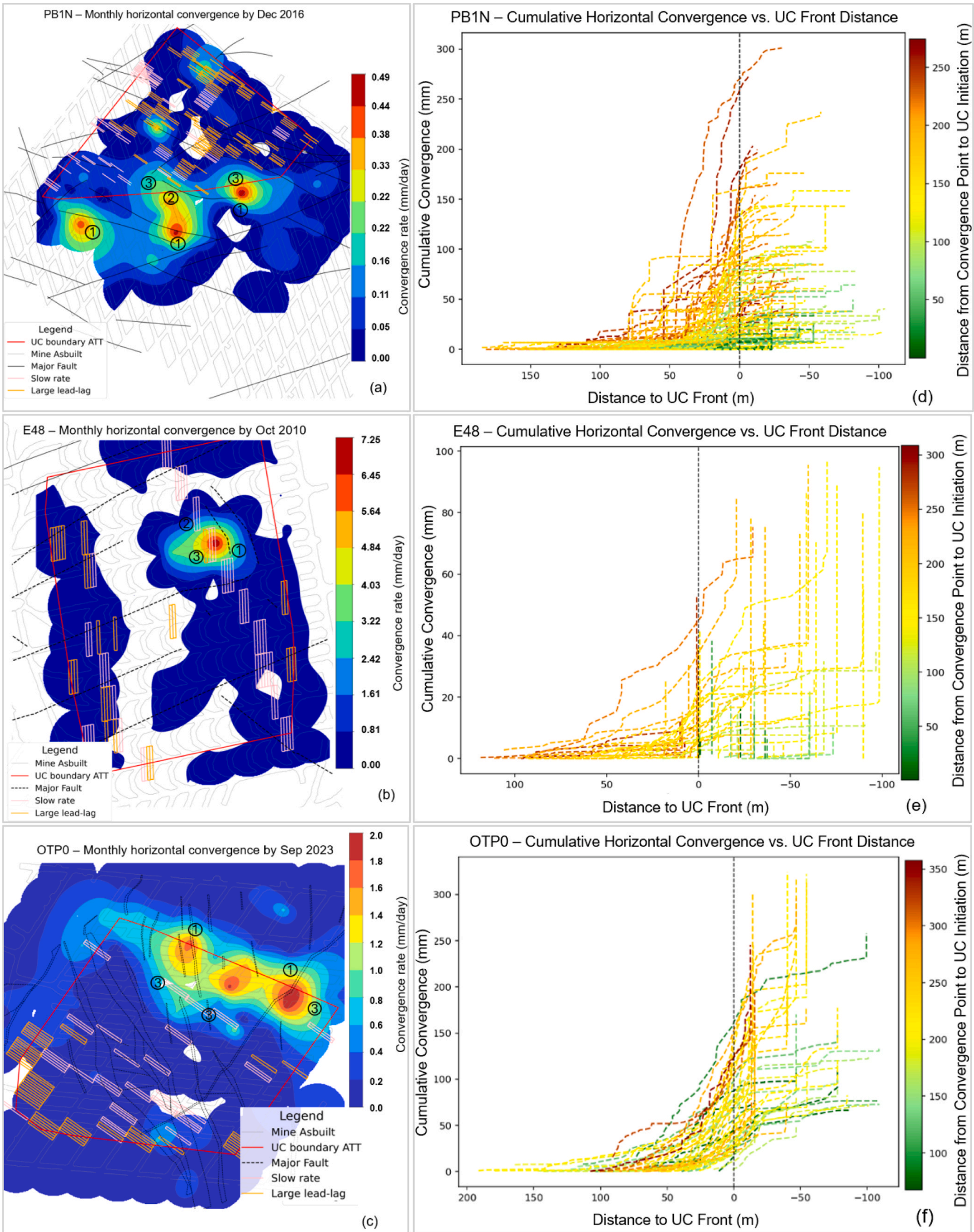

Fig. 12. Exemplary of monthly displacement contour maps highlighting zones of highest displacement close to (1) geological structures; (2) large lead-lag; or (3) slow UC advance rate for (a) DMLZ-PB1N, (b) E48, and (c) OTP0. Cumulative displacement curves are plotted relative to the UC front distance and colour-coded by the distance between each monitoring point and the UC initiation point, shown in (d) DMLZ-PB1N, (e) E48, and (f) OTP0.

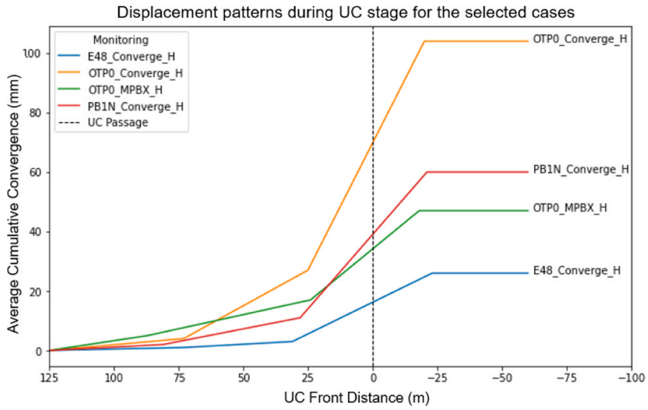

Fig. 13. Horizontal displacement patterns during undercutting in three cases, excluding monitoring data around cave boundaries.

4.2. *Displacement rate changes during undercutting*

During undercutting, horizontal displacements were dominant, and similar trends were observed across all three case studies. Displacement typically initiated approximately 75–80 m ahead of the UC front, accelerated around 25–30 m before the UC front passed over, and stabilised about 20–25 m behind the front after its passage (Fig. 13).

OTP0 MPBX data showed minimal vertical displacement before undercutting, whereas E48 exhibited simultaneous vertical and horizontal displacement during undercutting (Fig. 14).

In terms of displacement rate and magnitude, all three cases showed a consistent trend of increasing horizontal displacement rates as the UC area expanded. It is important to note that this comparison is based solely on consistent monitoring data collected during the undercutting stage (Fig. 15).

A clear correlation was observed between areas of high displacement during undercutting and subsequent rehabilitation or PSM implementation. The most significant ground deformations occurred in regions that recorded high displacement during the UC passes (Fig. 16).

5. Discussion

It is important to note that the magnitude of the rock mass displacements in the three case studies cannot be directly compared due to their unique geological, geotechnical and mining conditions, including differences in their virgin stress state, undercutting geometry, UC method, front rates, and ground support designs. However, the trends and patterns of their ground displacements during undercutting can be compared using their continuous monitoring data recorded over the

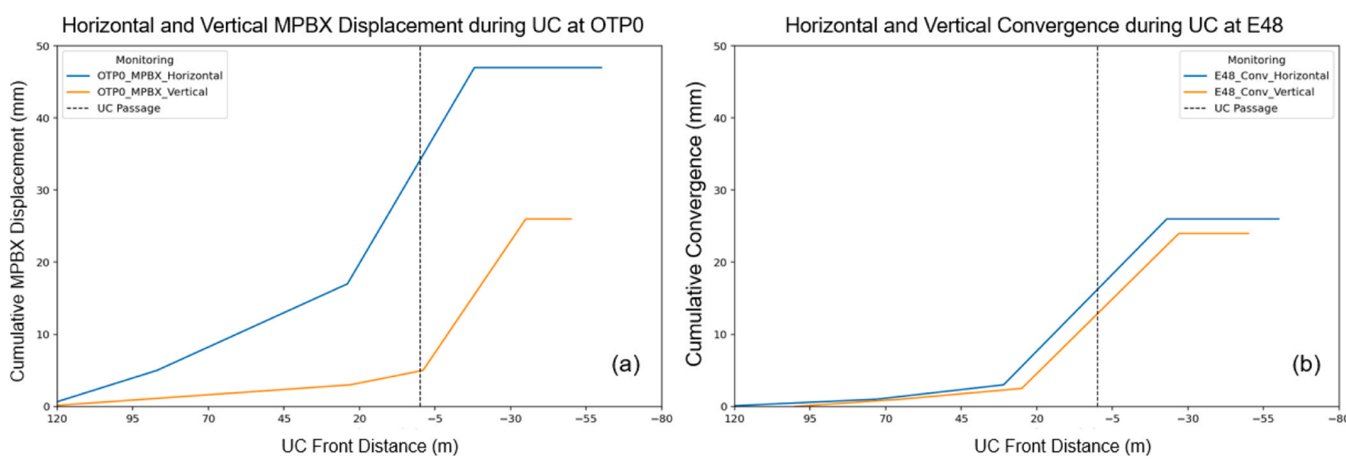

Fig. 14. Horizontal and vertical displacement patterns during undercutting in (a) OTP0 and (b) E48.

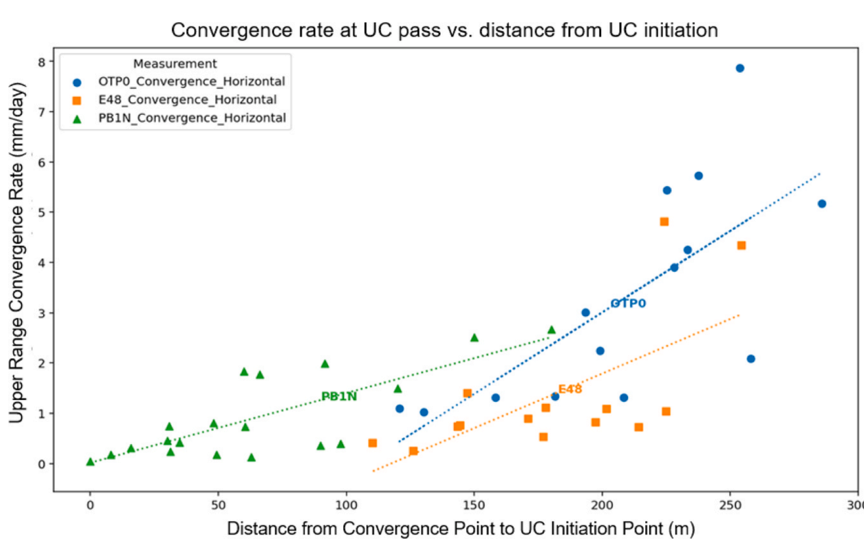

Fig. 15. Scatter plot illustrating the relationship between convergence rates measured at monitoring points during UC front pass-over and their distances from the UC initiation location for the three cases.

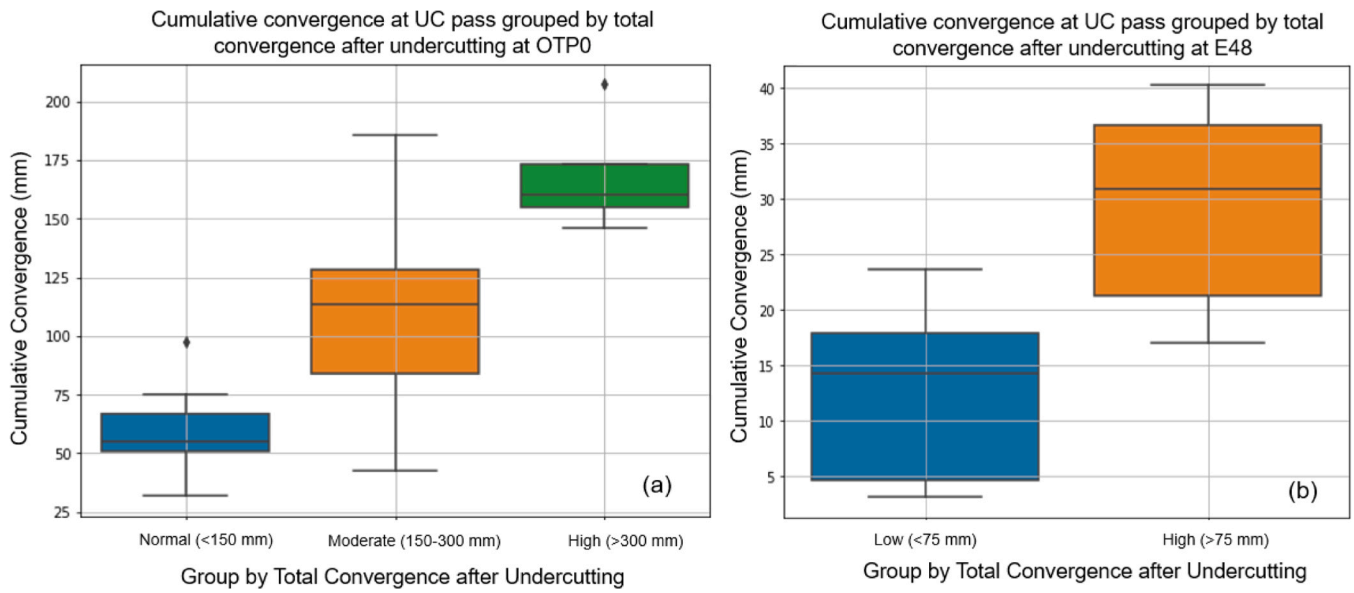

Fig. 16. Boxplot showing cumulative convergence during UC front pass-over at different locations, grouped by their total convergence levels after undercutting at (a) OTP0 and (b) E48.

entire undercutting stage.

5.1. Interpretation for deformation data analysis

The increase in displacement near the UC front is likely due to high abutment stress concentrations, consistent with observations in other deep cave mines. This suggests that UC geometry and sequencing play a critical role in localising deformation.

- Typically, all three cases showed that their highest displacements during the UC stage correlated spatially with the location of structural features or areas where the UC was delayed. This can be attributed to the fact that structural features generally exhibit lower strength compared to intact rock masses, making them more susceptible to deformation under high abutment stress.
- The trend of higher displacement around the UC front with increasing UC area suggests that the induced stress from undercutting intensifies as the UC area expands. As a result, depending on the rock mass strength, larger displacements and higher displacement rates are observed under increased loading conditions. This phenomenon highlights the potential value of evaluating an optimal UC area based on detailed rock mass data.
- In PB1N, a high horizontal displacement rate was initiated farther (35–80 m) ahead of the UC front in the later stages of undercutting, likely due to the longer UC front length and consequent slower UC advance rate.
- In OTP0, continuous displacement was observed around static cave boundaries, likely due to weak rock masses under high stress and prolonged cave propagation of block caving.

- The difference in the timing of the vertical displacement initiation is most likely related to the undercutting method; the E48 cave adopted a post-undercut, with vertical displacements occurring well ahead of the UC front, where drawpoints and drawbells had already been developed prior to undercutting.

5.2. Limitations in UC data analysis

Although displacement monitoring and UC blasting data enabled a detailed investigation of the ground response to undercutting, the analysis was constrained by the continuity and frequency of the available monitoring data. The main limitations of this observational analysis:

- **Displacement contouring** only represents the available measurements, resulting in gaps in contour maps where monitoring data is missing over the desired time windows.
- **Rate of change detection** excluded monitoring data with prolonged measurement interruptions during the undercutting stage,
- **Variability in displacement patterns**: Whilst the rate of change detection revealed clear patterns in the rock displacements during undercutting, significant variability was observed in the distance to the UC front and the magnitude of the displacements within the identified displacement zones (i.e. the displacement initiation ahead of the UC front, high displacement rates experienced during the UC advance, and the displacement stabilisation after the UC had passed over). These variations are likely influenced by factors such as the mucking/drawing rates implemented during undercutting and the local rock mass conditions.
- **Excluded influencing factors**: Whilst the study focused on key UC parameters, namely the major geological structures, UC rate, and UC lead-lag distances, other known factors, such as the shape of the UC front and UC veranda length, were not considered.

6. Conclusions

Despite the high variability in rock mass characteristics and stress conditions across the selected cases, deformation data analysis supports previous studies, showing consistent trends and patterns in ground response during the undercut stage. While the magnitude of displacement and failure mechanisms varied, higher displacement distribution was consistently associated with key contributing factors, including UC area size, UC front length, UC rate, and the presence of structural features. These findings highlight the predictable nature of ground response to undercutting and emphasise the need for tailored, site-specific UC strategies, including:

- Optimising UC sequencing to reduce excessive deformation.
- Expanding monitoring coverage to strengthen PSM strategies and ground support planning.

Future work should prioritise integrating monitoring data with rock mass characterisation, identifying key influencing factors (including undercut method and undercut-front geometry), and improving predictive tools to support safer and more effective undercutting in deep, high-stress cave mines.

CRediT authorship contribution statement

Batbayar Batkhuu: Writing – original draft, Methodology, Formal analysis. **Andre van As:** Writing – review & editing, Supervision, Resources.

Declaration of Competing Interest

The authors declare no conflict of interest. The author Batbayar Batkhuu is a Guest Editor for the journal *Deep Resources Engineering* and was not involved in the editorial review or the decision to publish this article. The authors declare the following financial interests/personal relationships which may be considered as potential competing interests: The original research was funded by Oyu Tolgoi International Scholarship Program. The author Batbayar Batkhuu is an employee of Oyu Tolgoi LLC, Mongolia.

Acknowledgments

This study was supported by Oyu Tolgoi International Scholarship Program.

Data availability statement

Due to the sensitive nature of the questions asked in this study, survey respondents were assured raw data would remain confidential and would not be shared.

References

[1] D. Laubscher, A practical manual on block caving: Report to the Internal Caving Study (1997-2000), JKMRC and Itasca Consulting Group, Inc, Brisbane, 2000.
[2] J. Roy, A. Primadiansyah, E. Eberhardt, et al., Abutment loading in deep cave mines: Towards understanding susceptibility to strainbursts, Caving 2022. Proceedings of the Fifth International Conference on Block and Sublevel Caving, Australian Centre for Geomechanics, Perth, 2022, pp. 1121–1134.
[3] F. Fernandez, G. Watt, J. Ooi, Strategic management for squeezing ground conditions at the Argyle Diamonds block cave project, Strategic versus Tactical 2011. Proceedings of the Fourth International Seminar on Strategic versus Tactical Approaches in Mining, Australian Centre for Geomechanics, Perth, 2011, pp. 55–72.
[4] P. Brenchley, L. Snyman, J. Samosir, Redevelopment support at Northparkes Mines, Ground Support 2013. Proceedings of the Seventh International Symposium on Ground Support in Mining and Underground Construction, Australian Centre for Geomechanics, Perth, 2013, pp. 451–460.
[5] C. Kamp, Management of production drift convergence and redevelopment, Caving 2022. Proceedings of the Fifth International Conference on Block and Sublevel Caving, Australian Centre for Geomechanics, Adelaide, 2022, pp. 831–848.
[6] E.T. Brown, Julius Kruttschnitt Mineral Research Centre. Block caving geomechanics, The University of Queensland, Brisbane, 2003, p. 323.
[7] E. Rojas, R. Molina, A. Bonani, et al., The pre-undercut caving method at the El Teniente mine, Codelco Chile, in: MassMin, Australian Institute of Mining and Metallurgy, Brisbane, 2000, pp. 261–266.
[8] C. Brumleve, M. Maier, Applied investigation of rock mass response to panel caving, Henderson mine, Colorado, USA, in: D.R. Stewart (Ed.), Design and Operation of Caving and Sublevel Caving Mines, Society of Mining Engineers of the American Institute of Mining, Metallurgical, and Petroleum Engineers, New York, 1981, pp. 223–249.
[9] J. Lett, Geotechnical lessons learnt during undercutting in deep caving at Cadia Operations, Deep Mining 2024. Proceedings of the 5th International Conference & Exhibition on Mass Mining, Australian Centre for Geomechanics, Montreal, 2024, pp. 109–136.
[10] M. Barraza, P. Crorkan, Esmeralda mine exploitation project, in: MassMin, Australian Institute of Mining and Metallurgy, Brisbane, 2000, pp. 267–278.
[11] O. Araneda, A. Sougarret, Lessons learned in cave mining at the El Teniente mine over the period 1997-2007, MassMin 2008. Proceedings of the 5th International Conference & Exhibition on Mass Mining, Luleå University of Technology, Luleå, 2008, pp. 43–52.
[12] C.R. Pardo Mella. Back analysis of intensive rock mass damage at the El Teniente mine, PhD Thesis, Curtin University, Perth, 2015.
[13] L. Snyman, S. Webster, Northparkes E48 block cave: The mining history of a successful block cave, Caving 2022. Proceedings of the Fifth International Conference on Block and Sublevel Caving, Australian Centre for Geomechanics, Perth, 2022, pp. 95–108.
[14] P.P. Angin, R.K. Wattimena, D.P. Sahara, et al., Microseismic analysis to identify stress redistribution and minimize rockburst in DMLZ cave abutment, PT Freeport Indonesia, in: 5th ISRM Young Scholars' Symposium on Rock Mechanics and International Symposium on Rock Engineering for Innovative Future, ISRM, Okinawa, 2019, ISRM-YSRM-2019-154.
[15] K. Simanjuntak, A. Primadiansyah, N. Soumilena, et al., Driving and managing stress in the Deep Mill Level Zone caving mine, MassMin 2020. Proceedings of the Eighth International Conference & Exhibition on Mass Mining, University of Chile, Santiago, 2020, pp. 394–405.
[16] M. Napitupulu, M. Ali, E. Satriawan, et al., Preventive support maintenance (PSM) as a mitigation of rockburst hazard: A case study for the deep mill level zone mine, Society for Mining, Metallurgy & Exploration, 2022.
[17] J. Roy, E. Eberhardt, R. Bewick, et al., Application of data analysis techniques to identify rockburst mechanisms, triggers, and contributing factors in cave mining, Rock Mech. Rock Eng. 56 (4) (2023) 2967–3002.
[18] R. McMillan, Empirical analysis of brittle rock mass failure in response to undercut advance for preventive support maintenance, MASc Thesis, University of British Columbia, Vancouver, 2022.
[19] J. Ooi, G. Watt, H. Grobler, Raisebore stability and support at deep depth and highly defected rock mass condition: Oyu Tolgoi case study, Caving 2022. Proceedings of the Fifth International Conference on Block and Sublevel Caving, Australian Centre for Geomechanics, Perth, 2022, pp. 891–906.
[20] D. Laubscher, A geomechanics classification system for the rating of rock mass in mine design, J. South. Afr. Inst. Min. Metall. 90 (10) (1990) 257–273.
[21] Z. Bieniawski, The geomechanics classification in rock engineering applications, in: 4th ISRM Congress, Montreux, Switzerland (1979) ISRM-4CONGRESS-1979-117.
[22] ISRM, Suggested methods for monitoring rock movements using borehole extensometers, Int. J. Rock Mech. Min. Sci. Geomech. Abstr. 15 (6) (1978) 305–317.
[23] MDT, MPBX User Guide. Mine Design Technologies, Ontario, 2018.
[24] Surfer, A basic understanding of Surfer Gridding Methods – Part 1. Golden Software Support 2024.⟨https://support.goldensoftware.com/hc/en-us/articles/231348728-A-Basic-Understanding-of-Surfer-Gridding-Methods-Part-1#rbf⟩.
[25] C.F. Jekel, G. Venter, pwlf: A python library for fitting 1D continuous piecewise linear functions (2019). ⟨https://github.com/cjekel/piecewise_linear_fit_py⟩.

Batkhuu Batbayar completed his Master of Philosophy in Mining and Geotechnical Engineering at The University of Queensland, Australia, where he focused on ground response analysis and undercutting strategies in deep and high-stress cave mines. His research interests include geomechanical monitoring, rock mass characterisation in deep mines, stress-induced ground deformation, and the optimisation of cave establishment in caving operations.

Prof. Andre van As is an internationally recognised underground mine geotechnical engineer with over 30 years' experience specialising in cave mining geomechanics, cave management, and enabling technologies. He has held senior global leadership roles at Rio Tinto, pioneered the application of hydraulic fracturing for cave induction, and is currently Professor and Group Lead for Deep Mining Geoscience at the University of Queensland, while continuing to advise major cave mining operations worldwide.